A Study on the Physical Layer Performance of GFDM for High Throughput Wireless Communication

Ahmad Nimr, Dan Zhang, Ana-Belen Martinez and Gerhard Fettweis
Vodafone Chair Mobile Communication Systems, Technische Universität Dresden, Germany
{first name.last name}@ifn.et.tu-dresden.de

***Abstract*—In this paper, we investigate the physical layer (PHY) performance of generalized frequency division multiplexing (GFDM) for high throughput wireless communication. For comparison purposes, orthogonal frequency division multiplexing (OFDM)-based IEEE 802.11ac PHY is used as a benchmark. Harnessing the flexibility of GFDM, we propose a novel configuration, being compliant to the IEEE 802.11ac PHY for data transmission. With that configuration, we can achieve not only lower out-of-band (OOB) emission performance but also higher spectral efficiency. By further deriving the corresponding receiver, the overall GFDM-based PHY implementation is shown to attain better frame error rates (FERs) under various modulation and coding schemes (MCSs). Moreover, at the signal to noise ratios (SNRs) where the target FER of 10% is fulfilled, GFDM can also provide higher throughput than OFDM.**

I. Introduction

In the last years, IEEE 802.11 wireless local area network (WLAN) technologies have been evolving continuously. Due to their flexibility, low cost and easy of deployment compared to wired networks, they become more and more popular for both private and business use in the daily life. Therefore, they need to accommodate the increasing demand on data traffic for heterogeneous services.

The member IEEE 802.11ac [1] in the WLAN family targets high throughputs. Orthogonal frequency division multiplexing (OFDM) [2] is the waveform adopted by the IEEE 802.11ac physical layer (PHY). Given its high out-of-band (OOB) [3] emission, the subcarriers close to the edges of each band have to be disabled, thereby degrading the spectral efficiency. Targeting higher spectral efficiency, this paper aims at investigating the waveform aspect of the PHY for high throughput communication.

Generalized frequency division multiplexing (GFDM) [4] is a new waveform with high spectral efficiency and low OOB. Making use of its flexibility, it can be configured to work in compliance with the IEEE 802.11ac. The lower OOB emission of GFDM allows to reduce the number of guard subcarriers used in OFDM. These subcarriers can be used for data transmission, increasing the throughput. Additionally, GFDM can be configured to work on a symbol basis, namely, multiple data symbols per subcarrier. Using one cyclic prefix (CP) to protect multiple data symbols per subcarrier, we can save time resources. In this particular case, two CP-OFDM symbols are combined into one GFDM symbol. The time resource corresponding to the saved CP is reused by inserting a training sequence to track the common phase error (CPE) caused by the residual carrier frequency offset (CFO). To our best knowledge, this is the first work in the literature that investigates the waveform aspect of IEEE 802.11ac for an improved PHY performance.

The reminder of the paper is organized as follows: Section II provides a review of GFDM modulation. In Section III, we propose the configuration and waveform design of GFDM for 802.11ac. The receiver design is presented in Section IV while evaluation and simulation results are represented in Section V. Finally, we conclude the paper in Section VI.

II. GFDM overview

GFDM is a symbol-based multicarrier modulation technique that employs circular filtering [4]. The available bandwidth B is divided into K subcarriers with subcarrier spacing $\Delta f = \frac{B}{K}$. Each subcarrier consists of equally spaced M subsymbols with time duration $T_{\text{sub}} = \frac{1}{\Delta f} = \frac{K}{B}$. Therefore, the duration of one GFDM symbol is equal to $T = MT_{\text{sub}} = \frac{N}{B}$, $N = MK$. Each pair of (k, m)-subcarrier and subsymbol can be used to transmit one data symbol $d_{k,m}$ modulated by a circular pulse shape $g_{k,m}(t)$ given by

$$g_{k,m}(t) = w_T(t) g_T(t - mT_{\text{sub}}) e^{j2\pi k \Delta f t}, \tag{1}$$

where, g_T is a periodic pulse shape of period T, and $w_T(t)$ is rectangular window, where $w_T(t) = 1,\ t \in [0,\ T]$ and 0 elsewhere. Let $\mathcal{K}_x$ and $\mathcal{M}_x$ be the sets of active subcarriers and subsymbols, respectively. The signal corresponding to the i-th GFDM symbol is denoted as

$$x_i(t) = \sum_{m \in \mathcal{M}_x} \sum_{k \in \mathcal{K}_x} d_{k,m,i} g_{k,m}(t). \tag{2}$$

Then, the signal of a frame, which contains I blocks, can be expressed as $x(t) = \sum_{i=0}^{I-1} x_i(t - iT)$. GFDM commonly adopts CP of duration $T_{\text{cp}} \geq \tau_{\max}$ to tackle the impact of fading channel with maximum excess delay spread $\tau_{\max}$. Then the window becomes $w_{T+T_{\text{cp}}}(t)$.

The discrete time signal representation can be derived from the critical sampling of the analogue signal with frequency $F_s = B$. With that, we get K, N and N_{cp} samples per

ISBN 978-0-9928626-7-1

subsymbol, symbol and CP, respectively. The i-th block can be represented in a vector $\boldsymbol{x}_i \in \mathbb{C}^{N\times 1}$, such that,

$$[\boldsymbol{x}_i]_{(n)} = \sum_{m\in\mathcal{M}_x}\sum_{k\in\mathcal{K}_x} d_{k,m,i}\, g[< n - mK >_N] e^{j2\pi\frac{k}{K}n}. \quad (3)$$

The block with CP is represented by coping the last N_{cp} samples to the beginning of $\boldsymbol{x}_i$. The matrix representation can be written as $\boldsymbol{x}_i = \boldsymbol{A}\boldsymbol{d}$, $[\boldsymbol{d}]_{(k+mK)} = d_{k,m},\ (k,m)\in\mathcal{K}_x\times\mathcal{M}_x$ and 0 elsewhere. $\boldsymbol{A}\in\mathbb{C}^{N\times N}$ is the modulation matrix, $[\boldsymbol{A}]_{(n,k+mK)} = g[< n-mK >_N] e^{j2\pi\frac{k}{K}n}$. The set of allocated resources is defined as

$$\mathcal{N}_x = \{n = k + mK,\ (k,m)\in\mathcal{K}_x\times\mathcal{M}_x\}, \quad (4)$$

$$\text{then, } \boldsymbol{x}_i = \boldsymbol{A}^{(x)}\boldsymbol{d}^{(x)}, \quad (5)$$

where $\boldsymbol{A}^{(x)} = [\boldsymbol{A}]_{(:,\mathcal{N}_x)}$ and $\boldsymbol{d}^{(x)} = [\boldsymbol{d}]_{(\mathcal{N}_x)}$.

III. 802.11AC BASED GFDM CONFIGURATION

In this work, we consider GFDM as an alternative waveform for the payload of the 802.11ac frame. The same preamble is used for time and frequency synchronization and channel estimation, Fig. 1.

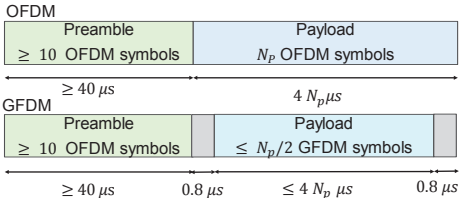

Fig. 1: Proposed GFDM vs OFDM frame structure.

For the OFDM configuration [1], the subcarrier spacing is fixed to $\Delta f = 312.5$ kHz, which corresponds to a useful symbol duration $T = 3.2$ μs. The CP duration is one quarter of T, i.e. $T_{\text{cp}} = 0.8$ μs. Thus, the total symbol duration equals $T_{\text{sym}} = 4$ μs. By using K_{ofdm} subcarriers, the number of samples per symbol is equal to $K_{\text{ofdm}} + N_{\text{cp}}$. A set of subcarriers $\mathcal{K}_d$ is used to transmit data symbols $\boldsymbol{d}_i^{(d)}$, and another set $\mathcal{K}_p$ is used to transmit pilot symbols $\boldsymbol{d}_i^{(p)}$.

In the proposed GFDM configuration, the GFDM symbol has no CP. Instead an approximately fixed tail of length $N_{\text{tail}} = N_{\text{cp}}$ is used to play the role of CP. In this way, the tail of the $(i-1)$-th symbols is used as CP for the i-th symbol, as illustrated in Fig. 2. However, the fixed tail needs to be added to the beginning of the frame.

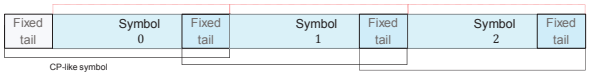

Fig. 2: Fixed tail approach.

By exploiting the fact that $N_{\text{cp}} = K_{\text{ofdm}}/4$, we set $K = K_{\text{ofdm}}/4$ to have a subsymbol duration equal to N_{cp}. Accordingly, the subcarrier spacing of GFDM is 4 times wider. Considering a well-localized prototype pulse shape within two subsymbols spacing, i.e. $g[n]\approx 0,\ K\le n\le N-K-1$, then for $m = 1,\cdots M-2$, $g_{k,m}[n] = g[< n-mK >_N] \approx 0,\ n = N-K,\cdots,N-1$. This means that the tail of K samples is null, as illustrated in Fig. 3, where a raised-cosine (RC) pulse shape with roll-off factor $\alpha = 0.5$ is used. As a result,

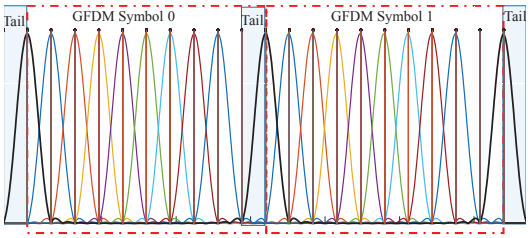

Fig. 3: GFDM waveform design. The first subsymbol (black curve) is a periodic pilot signal.

the set of subsymbols $\mathcal{M}_d = \{1,\cdots,M-2\}$ can be used for data transmission. Furthermore, the first subsymbol can be exploited to transmit a deterministic periodic pilot signal. This requires that the pilot subsymbols are fixed during the whole frame. With this configuration, the GFDM symbols have approximately a fixed tail equal to the last K samples of the pilot subsymbol. On the other hand, this design helps in reducing the OOB [4]. Moreover, to ensure smooth transition of the pilot signal, the first K samples of the GFDM pilot subsymbol are copied to the end of the frame. In order to guarantee the same throughput, it is required that $K|\mathcal{M}_d| \ge K_{\text{ofdm}}$. Hence, we take $M = 10$ to keep the GFDM symbol as short as possible. Consequently, the GFDM symbol duration is twice the OFDM one, as shown in Fig. 4.

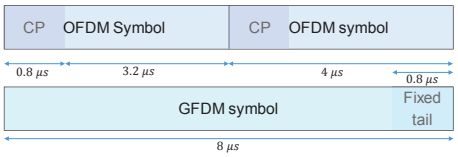

Fig. 4: GFDM vs OFDM symbol in 802.11ac.

Param.	OFDM	GFDM
Δf	312.5 kHz	1250 kHz
T_{sym}	4 μs (160 samples)	8 μs (320 samples)
K	128	32
M	1	10
$\mathcal{K}_d$	$\{-58,\cdots,58\}$ $\setminus\{0,\pm1\}\cup\mathcal{K}_p$	$\{-15,\cdots,14\}/\{0\}$
$\mathcal{K}_p$	$\{\pm53,\pm25,\pm11\}$	$\{-14,\cdots,13\}/\{0\}$
$\mathcal{M}_d$	$\{0\}$	$\{1,\cdots,8\}$
$\mathcal{M}_p$	$\{0\}$	$\{0\}$
$\lvert\mathcal{N}_d\rvert$	108	232
$\lvert\mathcal{N}_p\rvert$	6	27
$g_T(t)$	1	Periodic RC (α)

TABLE I: 802.11ac configuration for $B = 40$ MHz.

In addition to the subsymbols sets $\mathcal{M}_d$, and $\mathcal{M}_p = \{0\}$, $\mathcal{K}_d$ and $\mathcal{K}_p$ denote the subcarriers sets used for data and pilot symbols, respectively. As a result, the sets $\mathcal{N}_d$ and $\mathcal{N}_p$ are defined as in (4). Table I summarizes the detailed configuration for $B = 40$ MHz.

ISBN 978-0-9928626-7-1 © EURASIP 2017

The useful bit rate R depends on the payload size N_p and the modulation and coding schemes (MCSs). Besides the overhead of the preamble, another factor is the zero padding, which is required to fit the coded payload in an integer number of symbols. The overhead is larger for high MCSs, smaller payload and longer symbol, as illustrated in Fig. 5. It can also be shown that, for a given MCS and sufficiently big N_p, R becomes constant, $R \approx \frac{\mathbb{E}[N_P]}{\mathbb{E}[T_f(N_p)]}$. Here, $T_f(N_p)$ denotes the frame duration. As listed in Table. II, within the selected ranges of N_p, the GFDM gain is higher for lower MCSs, as well as when the payload is large.

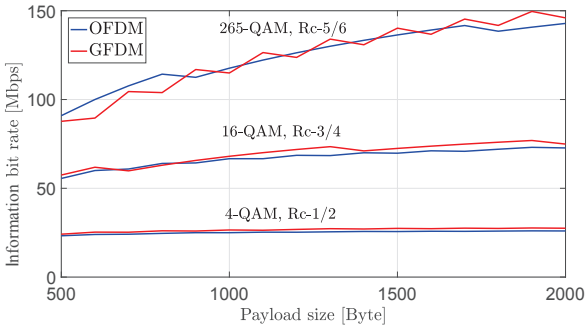

Fig. 5: PHY information bit rate vs payload size.

M QAM	R_c	N_P range [Byte]	R_G[Mpbs] GFDM	OFDM	GFDM gain
4	1/2	[500, 1000]	25.54	24.33	5.0%
16	3/4	[1000, 1500]	71.15	68.35	4.1%
256	5/6	[1500, 2000]	143.26	139.87	2.4%

TABLE II: MCSs settings.

IV. Transceiver Design

As depicted in Fig. 7, the transmitted signal of the payload is a superposition of data and pilot signals, which are allocated according to the sets $\mathcal{N}_d$ and $\mathcal{N}_p$[1]. Therefore, the i-th block can be written, following (5) as

$$\boldsymbol{x}_i = \boldsymbol{A}^{(d)}\boldsymbol{d}_i^{(d)} + \boldsymbol{A}^{(p)}\boldsymbol{d}_i^{(p)}. \tag{6}$$

The payload signal $x[n]$ is multiplexed with a preamble, to generate the transmitted signal $x_t[n]$, Fig. 1. The signal is transmitted via a fading channel with equivalent impulse response $h[l]$ of length L taps. The overall CFO of transmitter and receiver is denoted as f_o. Additive white noise $C\mathcal{N}(0, N_0)$ is added at the receiver. On the received signal $y_t[n]$, time and frequency synchronization is performed exploiting the preamble training frames, Fig 6, the legacy short training field (L-STF) [5], [6] and the legacy long training field (L-LTF) [7]. First, the frame is detected, the CFO is estimated and compensated and the reference symbol timing is found with residual time offset (TO) denoted as T_o. Afterwards, zero forcing channel estimation [8] is performed using L-LTF and

[1]This signal model can be used to describe both GFDM block and OFDM symbol. Thereby, the later derivations are applicable for both cases.

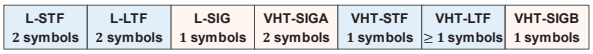

Fig. 6: OFDM based preamble.

the very high throughput (VHT)-LTF. Assuming $T_o \geq 0$ and $T_o + L - 1 \leq N_{cp}$, the estimated channel is equivalent to $\hat{h}[l-T_o]$. A residual phase noise ϕ_n remains after synchronization. Therefore, the payload received signal can be expressed as

$$y[n] = e^{j\phi_n} h[n - T_o] * x[n] + v[n], \tag{7}$$

where, $v[n]$ is the additive noise. The received block $\boldsymbol{y}_i$ is generated as $[\boldsymbol{y}_i]_{(n)} = y[n + N_{\text{cp}} + iN]$. Under the assumption $T_o + L - 1 \leq N_{cp}$, the linear convolution becomes circular [9]. However, in the case of the proposed fixed tail configuration, if the tail of the symbols are not exactly equal, additional interference appears. Therefore, $\boldsymbol{y}_i$ can be expressed as,

$$\boldsymbol{y}_i = \boldsymbol{\Phi}_i \boldsymbol{H}_c \boldsymbol{x}_i + \boldsymbol{z}_i^{(\text{tail})} + \boldsymbol{v}_i. \tag{8}$$

where, $\boldsymbol{\Phi}_i$ is a diagonal matrix generated from the phase noise, $\boldsymbol{H}_c$ the circular channel matrix, $\boldsymbol{z}_i^{(\text{tail})}$ the interference due to tail mismatch and $\boldsymbol{v}_i$ additive noise vectors. Taking N-DFT of (8) and replacing (6), we get

$$\tilde{\boldsymbol{y}}_i = e^{j\phi_i} \boldsymbol{\Lambda}^{(\hat{\tilde{h}})} \left(\tilde{\boldsymbol{A}}^{(d)} \boldsymbol{d}_i^{(d)} + \tilde{\boldsymbol{A}}^{(p)} \boldsymbol{d}_i^{(p)} \right) + \tilde{\boldsymbol{z}}_i^{(\text{tail})} + \tilde{\boldsymbol{z}}_i^{(\text{ICI})} + \tilde{\boldsymbol{v}}_i. \tag{9}$$

Here, $\tilde{\boldsymbol{x}} = N\text{-DFT}(\boldsymbol{x})$ and $\boldsymbol{\Lambda}^{(\tilde{h})} = \text{diag}\left\{\tilde{\boldsymbol{h}}\right\}$. The terms, $\tilde{\boldsymbol{z}}_i^{(\text{ICI})}$ and $e^{j\phi_i}$ denote the inter-carrier-interference (ICI) and CPE due to phase noise. As represented in [10], when ϕ_n is small, the phase noise effect after DFT transformation can be approximated by phase rotation, which is equal on all sub-carriers, and additional ICI. Defining $\tilde{\boldsymbol{A}}^{(p,d)} = \left[\tilde{\boldsymbol{A}}^{(p)}\ \tilde{\boldsymbol{A}}^{(d)}\right]$, $\tilde{\boldsymbol{z}}_i = \tilde{\boldsymbol{z}}_i^{(\text{tail})} + \tilde{\boldsymbol{z}}_i^{(\text{ICI})} + \tilde{\boldsymbol{v}}_i$, $\bar{\boldsymbol{d}}_i^{(p)} = e^{j\phi_i}\boldsymbol{d}_i^{(p)}$, and $\bar{\boldsymbol{d}}_i^{(d)} = e^{j\phi_i}\boldsymbol{d}_i^{(d)}$ we get

$$\tilde{\boldsymbol{y}}_i = \boldsymbol{\Lambda}^{(\hat{\tilde{h}})} \tilde{\boldsymbol{A}}^{(p,d)} \begin{bmatrix} \bar{\boldsymbol{d}}_i^{(p)} \\ \bar{\boldsymbol{d}}_i^{(d)} \end{bmatrix} + \tilde{\boldsymbol{z}}_i. \tag{10}$$

Assuming that $\tilde{\boldsymbol{z}}_i$ is dominated by the Gaussian noise vector $\tilde{\boldsymbol{v}}_i$, with variance N_0, and the data symbols and pilots are i.i.d. with variance E_s, the linear minimum mean square error (LMMSE) [11] equalization matrix $\boldsymbol{B}$ can be expressed as

$$\boldsymbol{B} = \left(\tilde{\boldsymbol{A}}^{(p,d)H} \boldsymbol{\Lambda}^{(\hat{\tilde{h}})H} \boldsymbol{\Lambda}^{(\hat{\tilde{h}})} \tilde{\boldsymbol{A}}^{(p,d)} + \frac{N_0}{E_s} \boldsymbol{I} \right)^{-1} \tilde{\boldsymbol{A}}^{(p,d)H} \boldsymbol{\Lambda}^{(\hat{\tilde{h}})H}. \tag{11}$$

The estimator of the rotated pilots and data symbols can then be found as,

$$\begin{bmatrix} \hat{\bar{\boldsymbol{d}}}_i^{(p)} \\ \hat{\bar{\boldsymbol{d}}}_i^{(d)} \end{bmatrix} = \begin{bmatrix} \boldsymbol{B}^{(p)} \\ \boldsymbol{B}^{(d)} \end{bmatrix} \tilde{\boldsymbol{y}}_i, \tag{12}$$

where $\boldsymbol{B}^{(p)} \in \mathbb{C}^{|\mathcal{N}_p| \times N}$ and $\boldsymbol{B}^{(d)} \in \mathbb{C}^{|\mathcal{N}_d| \times N}$ are the LMMSE filter matrices corresponding to the pilot and data symbols, respectively. This estimator can be implemented with low complexity, as proposed in [12]. By using the pilot knowledge,

ISBN 978-0-9928626-7-1 © EURASIP 2017

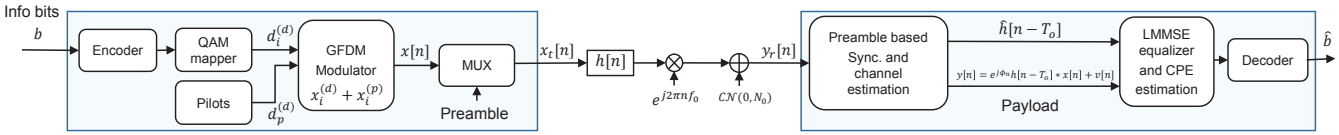

Fig. 7: Baseband transceiver block diagram.

we can estimate the phase rotation from the model,

$$\hat{\tilde{\boldsymbol{d}}}_i^{(p)} = e^{j\phi_i}\boldsymbol{d}_i^{(p)} + \boldsymbol{\epsilon}_i. \tag{13}$$

The additive noise $\boldsymbol{\epsilon}_i$ is characterized by the mean vector

$$\mathbb{E}\left[\boldsymbol{\epsilon}_i\right] = \mathbb{E}\left[\hat{\tilde{\boldsymbol{d}}}_i^{(p)} - e^{j\phi_i}\boldsymbol{d}_i^{(p)}\right] = \boldsymbol{b}_i, \tag{14}$$

where, $\boldsymbol{b}_i$ is the bias of the LMMSE estimator, $\boldsymbol{b}_i = \boldsymbol{B}^{(p)}\left(\boldsymbol{\Lambda}^{(\tilde{h})}\tilde{\boldsymbol{A}}^{(p)} - \boldsymbol{I}\right)\boldsymbol{d}^{(p)}e^{j\phi_i} + \boldsymbol{B}^{(p)}\boldsymbol{\Lambda}^{(\tilde{h})}\tilde{\boldsymbol{A}}^{(d)}\boldsymbol{d}^{(d)}e^{j\phi_i}$. The covariance matrix of $\boldsymbol{\epsilon}_i$ is given by

$$\boldsymbol{R}_{\epsilon_i} = \mathrm{cov}\left(\hat{\tilde{\boldsymbol{d}}}_i^{(p)}\right) = N_0\boldsymbol{B}^{(p)}\boldsymbol{B}^{(p)H}. \tag{15}$$

By using the best linear unbiased estimator (BLUE) [11], we get

$$\hat{\theta} = \frac{\boldsymbol{d}^{(p)H}\boldsymbol{R}_{\epsilon_i}^{-1}\left(\hat{\tilde{\boldsymbol{d}}}^{(p)} - \boldsymbol{b}_i\right)}{\boldsymbol{d}^{(p)H}\boldsymbol{R}_{\epsilon_i}^{-1}\boldsymbol{d}^{(p)}}. \tag{16}$$

Afterwards, the estimate of CPE can be achieved by $\hat{\phi}_i = \angle(\hat{\theta})$. Finally, the estimated data symbols $\hat{\boldsymbol{d}}$ are rotated by $-\hat{\phi}_i$ and fed to the decoder.

V. Simulation Results

We consider an OFDM 802.11ac based PHY in 40 MHz operation mode, Table I. We aim to compare its performance with our proposed GFDM based PHY. The PHY performance metrics of interest include: 1) power spectral density (PSD), 2) frame error rate (FER) and 3) throughput. First, the OOB emission is evaluated and demonstrated in Fig. 8 which depicts the PSD of the data signal $P_{x^{(d)}}$. As shown in the figure,

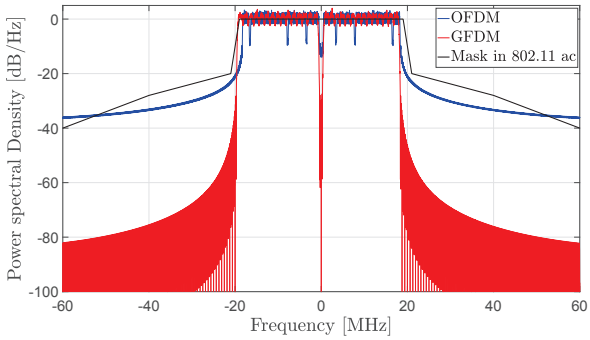

Fig. 8: PSD of data signal.

GFDM achieves ultra low OOB emission with the proposed configuration.

Next, we evaluate the FER, and throughput with respect to the signal to noise ratio (SNR) defined by[2]

$$\mathrm{SNR} = 10\log_{10}\left(\frac{\mathbb{E}\left[|x_t[n]|^2\right]}{N_0}\right)\ [\mathrm{dB}]. \tag{17}$$

Uniform power allocation is used among all active subcarriers and subsymbols. The channel under investigation follows the TGn Channel Model B [13], that has 9 Rayleigh delay taps, Table III, and Doppler shift $f_d = 3$ Hz. f_o is a random variable with uniform distribution in $[-233, 233]$ Khz. This range corresponds to an oscillator accuracy of 20 ppm at transmitter and receiver, with a maximum carrier frequency of 5.825 GHz. Synchronization, channel and CPE estimation are performed as discussed in Section IV. N_p is randomly selected with uniform distribution on the ranges given in Table II. Within the selected payload size range, the throughput can be calculated as $\mathrm{Th} = R \cdot (1 - \mathrm{FER})$.

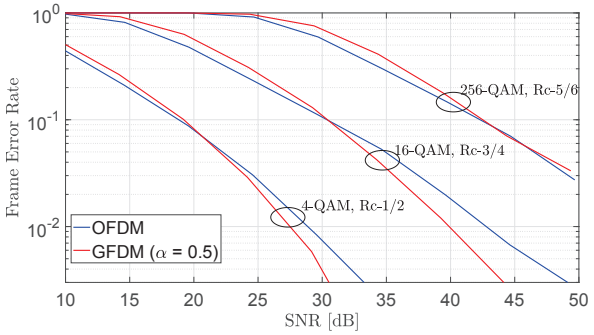

Fig. 9: FER vs SNR.

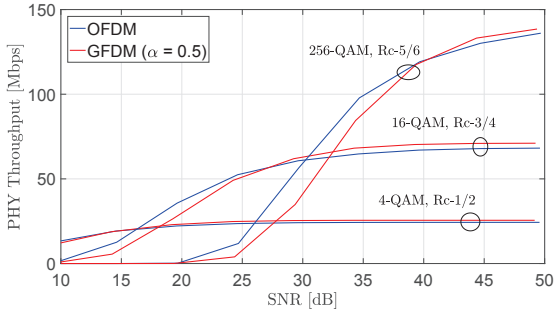

Fig. 10: PHY throughput vs SNR.

Fig. 9 and Fig. 10 illustrate the FER and the achievable throughput, respectively. GFDM outperforms OFDM significantly at higher SNRs and lower MCS, in terms of FER.

[2]Note, here our SNR represents the ratio between the power of the transmitted signal and noise. It is not equal to energy per symbol to noise ratio.

ISBN 978-0-9928626-7-1 © EURASIP 2017

Tap index	1	2	3	4	5	6	7	8	9
Excess delay [ns]	0	10	20	30	40	50	60	70	80
Power [dB]	0	−5.40	−2.50	−5.88	−9.15	−12.50	−15.60	−18.70	−21.80

TABLE III: TGn channel model B delay taps and gain. Doppler shift f_d = 3 Hz.

This allows GFDM to provide better throughput when the FER is above the threshold of 10%. With this condition, the throughput gain of GFDM ranges between $2-5\%$. For instance, with MCS 16- QAM and code rate $3/4$, the operating SNR to deliver FER below 10% is beyond 30dB, see Fig. 9. Accordingly, Fig. 10 shows that GFDM can deliver higher throughput than OFDM when SNR is larger than 30 dB. It is worth noting that both figures use the SNR as the channel quality measure. For GFDM, each GFDM symbol carries more data symbols than the OFDM symbol. Therefore, for a given SNR, the effective energy per data symbol in the GFDM case is smaller than that in the OFDM case. For this reason, the benefits of using GFDM are expected to be enlarged when energy per symbol to noise ratio is the channel quality measure.

In Fig. 11, we compare the effect of tail mismatch on the performance. For bigger α, RC becomes more localized in time. Therefore, the tail mismatch interference decreases. As can be seen from the figure, the effect appears only at higher SNRs and MCS, where the interference due to tail mismatch is dominant over the noise. Nevertheless, the error floor only takes place when the FER is already below 10%.

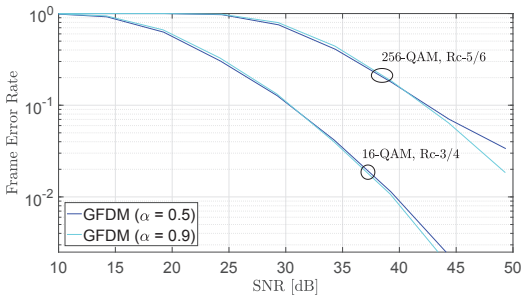

Fig. 11: FER acheived by GFDM with different roll-off factors.

VI. Conclusion

The specifications imposed by the new generations of wireless communications drive the research of innovative solutions which can cope with the current unresolved issues. In particular, the high OOB emission obtained with OFDM has to be reduced. GFDM appears as a flexible waveform that fulfills the requirements which OFDM cannot satisfy. In this paper, GFDM is configured and evaluated under the IEEE 802.11ac framework. By means of simulation, it is shown that GFDM presents a substantially lower OOB emission than OFDM. Simulations results indicate that, for the low, medium and high MCSs considered in this work, GFDM can achieve up to 5% gain in terms of throughput. Whereas the frame error rate (FER) is similar with high MCS for both waveforms, GFDM achieves a considerable lower FER for the other two cases, especially at higher SNRs.

The achieved gain of GFDM comes at the cost of increased complexity compared to OFDM based PHY. Nevertheless, the well-localization property in time and frequency of the pulse shaping allows efficient implementation of GFDM modem and advanced receiver algorithms.

Acknowledgment

This work was partly funded by the German Federal Ministry of Education and Research (BMBF) under grant 16KIS0250 (project: proWiLAN). The authors would like to thank the Horizon 2020 project ICT-688116 "eWINE" for partially funding the works. We also thank the reviewers for their constructive comments and remarks.

References

[1] "Part 11: Wireless LAN Medium Access Control (MAC) and Physical Layer (PHY) Specifications. Amendment 4: Enhancements for Very High Throughput for Operation in Bands below 6 GHz. IEEE Std 802.11ac-2013," Dec 2013.

[2] J. A. Bingham, "Multicarrier modulation for data transmission: An idea whose time has come," *IEEE Commun. Mag.*, vol. 28, no. 5, pp. 5–14, 1990.

[3] J. Van de Beek and F. Berggren, "Out-of-band suppresssion in OFDM," *IEEE Commun. Lett.*, vol. 55, no. 9, pp. 609–611, Sep 2014.

[4] N. Michailow *et al.*, "Generalized frequency division multiplexing for 5th generation cellular networks," *IEEE Trans. Commun.*, vol. 62, no. 9, pp. 3045–3061, Sep 2014.

[5] M. J. Canet *et al.*, "FPGA implementation of an OFDM-based WLAN receiver," *Microprocess. Microsyst.*, vol. 36, no. 3, pp. 232–244, May 2012. [Online]. Available: http://dx.doi.org/10.1016/j.micpro.2011.11.004

[6] H. Song *et al.*, "Frequency-Offset Synchronization and Channel Estimation for OFDM-Based Transmission," *IEEE Communications Letters*, vol. 45, no. 4, pp. 95–97, Mar 2000.

[7] A. B. Awoseyila *et al.*, "Robust time-domain timing and frequency synchronization for OFDM systems," *IEEE Transactions on Consumer Electronics*, vol. 55, no. 2, pp. 391–399, May 2009.

[8] V. D. Beek *et al.*, "On channel estimation in OFDM systems," in *Vehicular Technology Conference, 1995 IEEE 45th*, vol. 2. IEEE, 1995, pp. 815–819.

[9] J. Heiskala and J. Terry Ph D, *OFDM wireless LANs: A theoretical and practical guide*. Sams, 2001.

[10] A. G. Armada, "Understanding the effects of phase noise in orthogonal frequency division multiplexing (OFDM)," *IEEE Trans. Broadcast.*, vol. 47, no. 2, pp. 153–159, 2001.

[11] S. M. Kay, "Statistical signal processing," *Estimation Theory*, vol. 1, 1993.

[12] D. Zhang, M. Matthé, and G. Fettweis, "A study on the link level performance of advanced multicarrier waveforms under MIMO wireless communication channels," accepted for publication in IEEE Trans. Wireless Commun.

[13] G. Breit *et al.*, "IEEE P802.11 Wireless LANs. TGac Channel Model Addendum," Mar 2009.